ORIGINAL ARTICLE

Physicochemical and nanomedicine applications of phyto-reduced erbium oxide (Er$_2$O$_3$) nanoparticles

Hamza Elsayed Ahmad Mohamed[1,2], Ali Talha Khalil[3]* , Khaoula Hkiri[1,2], Muhammad Ayaz[4]* , Jamil Anwar Abbasi[4], Abdul Sadiq[4], Farhat Ullah[4], Asif Nawaz[4], Ikram Ullah[5] and Malik Maaza[1,2]

Abstract

Hyphaene thebaica fruits were used for the fabrication of spherical erbium oxide nanoparticles (HT-Er$_2$O$_3$ NP$_S$) using a one-step simple bioreduction process. XRD pattern revealed a highly crystalline and pure phase with crystallite size of ~ 7.5 nm, whereas, the W–H plot revealed crystallite size of 11 nm. FTIR spectra revealed characteristic Er-O atomic vibrations in the fingerprint region. Bandgap was obtained as 5.25 eV using K-M function. The physicochemical and morphological nature was established using Raman spectroscopy, reflectance spectroscopy, SAED and HR-TEM. HT-Er$_2$O$_3$ NP$_S$ were further evaluated for antidiabetic potential in mice using in-vivo and in-vitro bioassays. The synthesized HT-Er$_2$O$_3$ NP$_S$ were screened for in vitro anti-diabetic potentials against α-glucosidase enzyme and α-amylase enzyme and their antioxidant potential was evaluated using DPPH free radical assay. A dose dependent inhibition was obtained against α-glucosidase (IC$_{50}$ 12 µg/mL) and α-amylase (IC$_{50}$ 78 µg/mL) while good DPPH free radical scavenging potential (IC$_{50}$ 78 µg mL^{-1}) is reported. At 1000 µg/mL, the HT-Er$_2$O$_3$ NP$_S$ revealed 90.30% and 92.30% inhibition of α-amylase and α-glucosidase enzymes. HT-Er$_2$O$_3$ NPs treated groups were observed to have better glycemic control in diabetic animals (503.66 ± 5.92*** on day 0 and 185.66 ± 2.60*** on day 21) when compared with positive control glibenclamide treated group. Further, HT-Er$_2$O$_3$ NP$_S$ therapy for 21 days caused a considerable effect on serum total lipids, cholesterol, triglycerides, HDL and LDL as compared to untreated diabetic group. In conclusion, our preliminary findings on HT-Er$_2$O$_3$ NP$_S$ revealed considerable antidiabetic potential and thus can be an effective candidate for controlling the post-prandial hyperglycemia. However, further studies are encouraged especially taking into consideration the toxicity aspects of the nanomaterial.

Keywords Er$_2$O$_3$, Green nanotechnology, Diabetes, α-glucosidase and α-amylase

*Correspondence:
Ali Talha Khalil
alitalha.khalil@lrh.edu.pk;
talhakhalil2019@gmail.com
Muhammad Ayaz
Ayazuop@gmail.com
[1] UNESCO UNISA Africa Chair in Nanoscience and Nanotechnology, College of Graduate Studies, University of South Africa, Pretoria, South Africa
[2] Nanoscience African Network (NANOAFNET), Materials Research Department, iThemba LABS, Cape Town, South Africa
[3] Department of Pathology, Lady Reading Hospital Medical Teaching Institution, Peshawar 25000 KP, Pakistan
[4] Department of Pharmacy, Faculty of Biological Sciences, University of Malakand, Dir (L), KPK, Chakdara 18000, Pakistan

[5] Department of Biotechnology & Genetic Engineering, Hazara University Mansehra, Mansehra, KP, Pakistan

Mohamed *et al. AMB Express*   (2023) 13:24

Page 2 of 14

Introduction

Advances in nanobiotechnology over the past few years have yielded exciting applications across different fields, especially in medicine and drug delivery (Chittaranjan Patra 2021; Khalil et al. 2021a). It has been well established that materials on the nanometer scale possess a unique surface area to volume ratio that provide peculiar characteristics like enhanced reactivity and higher efficacy (Mohamed et al. 2020a). Among the metallic nanoparticles; silver, gold, zinc, iron etc. are well studied for their biomedical and nanomedicine applications, however, the lanthanides rare earth oxides are not well-explored (Ovais et al. 2019, 2020). The lanthanides rare earth oxides are known for their distinctive features and therefore used in number of applications such as energy, catalysis, photonics, environment, solid state optoelectronics, telecommunications, solar cells etc. Nano rare earth oxides are anticipated as exciting materials attributed to the quantum confinement and shape specific attributes (Rahimi-Nasrabadi et al. 2017). Mostly research on rare earth oxides is usually centered on the evaluation of physical, electrical, optical properties (Diallo et al. 2016; Rajaji et al. 2019). Among them, trivalent erbium oxide nanoparticles (Er_2O_3 NPs) are considered as one of the fascinating materials for applications in physical and chemical sciences. It usually has a pinkish color and cubic structure. Er_2O_3 is known for its mechanical properties, stiffness, thermal and chemical durability, inertness and corrosion resistance. Mechanical strength of the Er_2O_3 is comparable to alumina and magnesia. Er_2O_3 is a wide bandgap material i.e., ~ 5.4 eV (Acikgoz et al. 2021; Azad and Maqsood 2014; Rajaji et al. 2019). Er_2O_3 nanomaterials have revealed excellent potential in applications related to the gas sensors, optical communication, phosphorus display monitors, imaging and photoelectrochemical water splitting materials (Mohammadi and Fray 2009; Radziuk et al. 2011). Previously, antibacterial activity of Er_2O_3 is also reported against different pathogens like *P. aeruginosa, E. faecalis, S. aureus* and *E. coli* (Dědková et al. 2017).

Various chemical and physical processes can be utilized for preparation of the metal oxide nanoparticles such as hydrolysis, hydrothermal, sol–gel, precipitation, pyrolysis, thermal decomposition, ball milling etc. Previously, Er_2O_3 NPs were synthesized using chemical precursor like erbium nitrate (Azad and Maqsood 2014). Other methods like chemical bath deposition, microemulsion, sonochemical synthesis, low-pressure metallorganic chemical vapor deposition (MOCVD), thermal decomposition, solvo-hydrothermal, sol–gel, radio frequency (RF) sputtering etc. have been published for the preparation of Er_2O_3 NPs (Losurdo et al. 2007; Nguyen et al. 2010; Pacio et al. 2021; Que et al. 2001; Rajaji et al.

2019; Tabanli et al. 2017). Hitherto, being effective, these processes have disadvantages such as the wet chemistry-based approaches can generate toxic waste while, the physical methods are energy intensive. Furthermore, nanoparticles synthesized using chemical approaches can have low biocompatibility that limits their applications in medicine (Ovais et al. 2021; Sani et al. 2021). Contrary to physico-chemical methods, biological synthesis provides a suitable, one-step and economical alternative to other conventional means. Biological materials like the extracts of medicinal plants can be used as reducing, stabilizing and capping agents for the preparation of metal-based NPs (Khalil et al. 2021b; Nasar et al. 2022).

Diabetes mellitus (DM), disorder of the glucose metabolism and associated with hyperglycemia as well as other complications like neuropathy, retinopathy, nephropathy, and micro and macrovascular complications (Arky 1982). Defects in the production, secretion and action of insulin are responsible for hyperglycemia (Booth et al. 2016). DM affects about five percent population worldwide and its occurrence is increasing at an alarming rate, and is also associated with number of other diseases (Rahim et al. 2019). There are about 450 million peoples around the world which are effected by DM which is estimated to effect 690 million people till 2044 (Cho et al. 2018). Broadly the disease has two types including Type-1 diabetes (T1DM) and Type-2 diabetes (T2DM) (Del Prete et al. 1977; Himsworth and Kerr 1939). Inhibitors of two vital enzymes including alpha-glucosidase and alpha-amylase implicated in gastrointestinal glucose absorption are considered as vital drug targets. These enzymes breakdown polysaccharides (starch) to glucose and the inhibition of these enzymes play an important role to reduce glucose absorption in the intestine (Gin and Rigalleau 2000). Beside these targets, scavenging excessive number of free radicals is important. These free radicals generated during metabolic processes are responsible for a series of human illnesses including atherosclerosis, immune system destruction, cancer, neurological disorders, heart disorders, cerebro-vascular diseases and metabolic disorders (Saeed et al. 2021). In DM, free radicals cause lipids peroxidation, glucose oxidation and glycation of proteins (non-enzymatic) leading to DM and its complications (Mir et al. 2019; Sadiq et al. 2020). Number of antioxidants which may be natural or synthetic are used and can be helpful in metabolic disorders management (Mahnashi et al. 2022b).

Herein, we have reported extracts modulated biosynthesis of HT-Er_2O_3 NPs for the 1st time by using plant extracts as bioreducing agents. Aqueous extracts of the edible fruit of *Hyphaene thebaica* (Egyptian Doum; gingerbread in English) was used as bioreducing agents. *H. thebaica* has well-established uses in the folkloric

Mohamed *et al. AMB Express*   (2023) 13:24

Page 3 of 14

medicines and have been reported for dyslipidemia, hypertension, haematuria, bleeding, diuretic, diaphoretic, lowering blood pressure etc. (Abdulazeez et al. 2019; Khalil et al. 2018). After characterization different bioassays were performed (in-vitro & in-vivo) for determination of their antioxidant and antidiabetic potential & their safety was evaluated. Fig. 1 indicate the general study design for the present research.

Materials and methods

H. thebaica processing

The fruit material of *H. thebaica* was purchased in Aswan (Egypt), and was verified from a plant taxonomist. Fruit material was rinsed with double distilled water to clean any potential particulate material and kept for shade drying. Later, the fruit material grounded to fine powder and stored in zipper bags. Aqueous extraction was performed
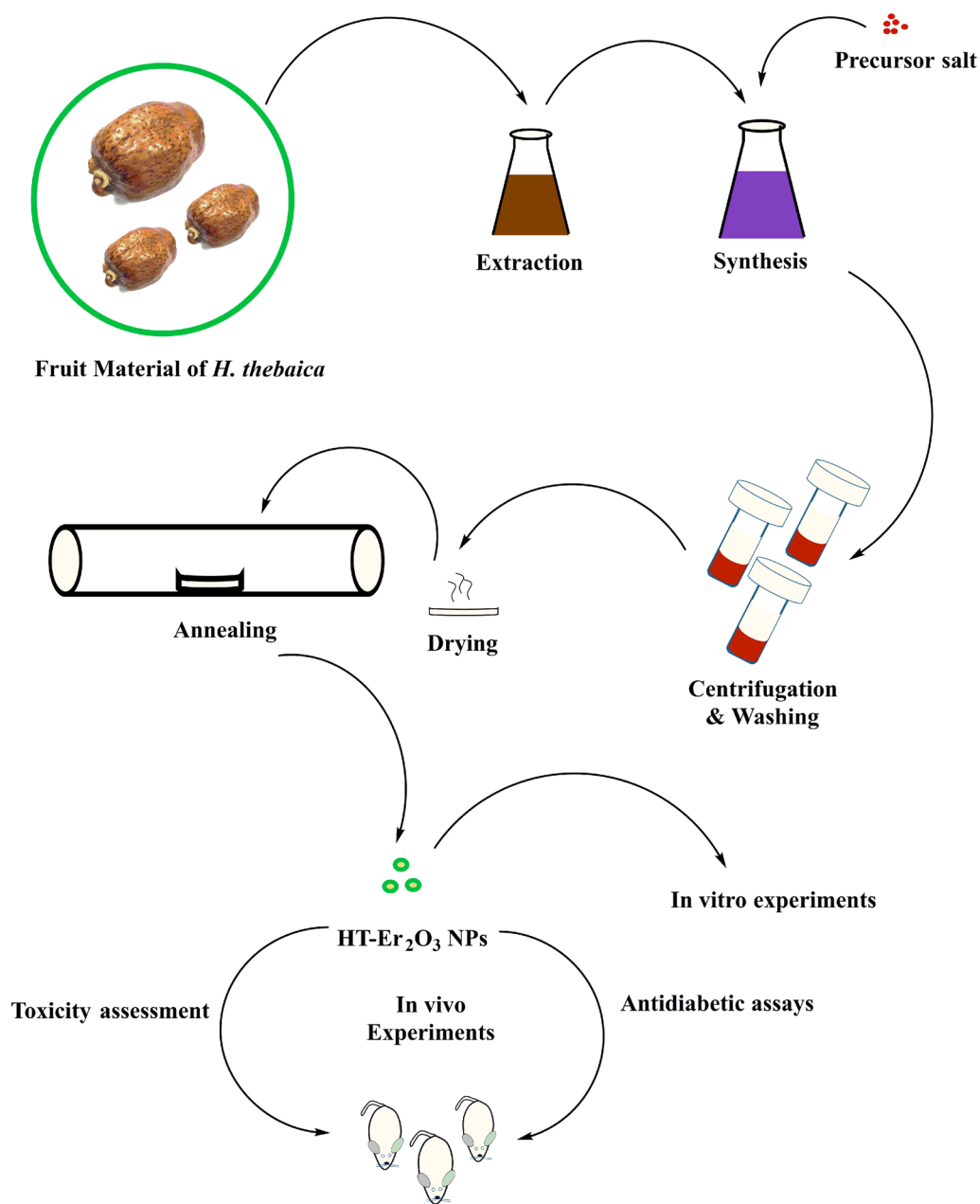

Fig. 1 Graphical scheme of study

Mohamed *et al. AMB Express* (2023) 13:24

Page 4 of 14

by heating 10 g powdered material in double distilled water (100 mL) for 1 h at 80 °C. Obtained mixture was cooled to room temperature and filtered three times for removing residual waste. The visually clear and transparent solution was used for synthesis.

Biosynthesis of HT-Er$_2$O$_3$ NPs

For biosynthesis, the precursor salt i.e. erbium nitrate (Er(NO$_3$)$_3$) (4 g) was introduced to 100 mL extract solution and allowed to stand room temperature for few minutes. Later, the solution was centrifuged at 8000 RPM for 20 min, and the pelleted precipitates were washed thrice in distil water. The washed precipitates were dried for 2 h (at 100 °C). Resultant powdered material (assumed as HT-Er$_2$O$_3$ NPs) was placed in the ceramic boat and calcinated for 2 h (500 °C) in a tube furnace.

Characterization

The physicochemical characteristics of the as synthesized NPs were analyzed via various techniques. XRD pattern was obtained to study the crystalline properties of HT-Er$_2$O$_3$ NPs. The x-ray diffractometer is equipped with Cu Kα (1.54 Å) radiation and the system is operating in Bragg–Brentano geometry The diffraction pattern was compared with the standard crystallography database and the crystallographic reflections were utilized to measure the average grain or crystallite size using Debye Scherrer approximation (Eq. 1) and Williamson-Hall equation (Eq. 2), as follows;

$$\langle D \rangle_{SIZE} = {K\lambda}/{\Delta\theta_{1/2}} \tag{1}$$

$$\beta\cos\theta = \left({K\lambda}/{D}\right) + 4\varepsilon\sin\theta. \tag{2}$$

here "λ" = 1.54 Å, and "K" = 0.9

The values of β cosθ were plotted as a function of 4 sinθ on the x-axis, followed by the linear fit for calculating the y-intercept and strain (ε) for obtaining the grain or crystallite size (D) using Williamson-Hall plot method (Zak et al. 2011). Furthermore, the dislocation density was determined using the formula (Bindu and Thomas 2014);

$$\delta = {1}/{D^2} \tag{3}$$

Where as; "δ" indicate dislocation density and "D" indicate grain or crystallite size of the nanoparticles.

The vibrational properties of the nanoparticles were studied by FTIR in the spectral range (4000 cm^{-1} to 400 cm^{-1}) and Raman spectra at room temperature with laser line 473 nm and average excitation power of 2.48 mW. Reflectance spectra was obtained in the range of 200 nm to 800 nm, and was used to obtain the optical bandgap using Kubelka–Munk function (Guler et al. 2015). High Resolution Transmission Electron Microscopy (HR-TEM) was performed to study the nanoparticles shape and morphology. Particle size distribution was obtained after processing the images using Image J. SAED pattern (Selected Area Electron Diffraction Pattern) was also obtained.

In-vitro experiments

Inhibition of alpha-glucosidase enzyme

The inhibitory potentials of Er$_2$O$_3$ NPs against alpha-glucosidase enzyme was evaluated according to protocol described previously with minor modification (Hussain et al. 2019). Commercially available enzymes were used in the study. Alpha-glucosidase (CAS 9001-42-7) used in the study was purchased from (sigma-Aldrich, USA). Glucosidase solution was prepared by dissolving α-glucosidase enzyme (0.5 μ/ml) in 120 μL of phosphate buffer with pH adjusted at 6.9. Buffer solution (0.1 M having pH 6.9) was used to prepare solution the enzyme substrate. Various serial samples dilutions were prepared ranging from 62.5 to 1000 μg mL^{-1} concentration were prepared. Initially, solution of enzyme was added to sample solution with subsequent incubation at 37 °C for 20 min. To this mixture, 20 μL of substrate solution was added and incubated again at the same temperature for fifteen minutes. To abort the reaction, 80 μL of Na$_2$O$_3$ solution was added to the mixture and the absorbance at 405 nm was recorded via spectrophotometer. Positive control was acarbose whereas, the blank one contained the same mixture without inhibitor agents. Finally, % α-glucosidase inhibitory results were calculated using our previously described procedure (Mahnashi et al. 2022b).

a-amylase inhibition

A-amylase inhibitory studies of the selected nanoparticles were performed as per the previously established procedure (Nair et al. 2013). Alpha-amylase from human saliva, Type XIII-A, lyophilized powder, 300–1500 units/mg protein (CAS 9000-90-2, EC 232-565-6) was obtained from Merck KGaA, Darmstadt, Germany. Briefly, α-amylase enzyme (20 μL) and 0.02 M sodium phosphate buffer (200 μL) was added to the test samples of different concentrations (31.25–1000 μg mL^{-1}), followed by 10 min incubation at room temperature and subsequent addition of starch (200 μl). 400 μL DNS (dinitrosalicylic acid) was added to stop the reaction, followed by boiling in water bath for 5 min and then allowed to cool. Finally,

Mohamed *et al. AMB Express*   (2023) 13:24

Page 5 of 14

15 mL double distilled water was introduced to the reaction mix and readings were recorded at 540 nm. No test sample was added the controls. Acarbose was utilized as standard α-amylase inhibitor.

DPPH-radicals scavenging assay

Anti-oxidant potential of HT-Er$_2$O$_3$ NPs (test compound) was determined by using 1,1-Diphenyl, 2-Picrylhydrazal (DPPH) (Dhanasekaran et al. 2015; Kamal et al. 2015). For making DPPH solution, 100 mL methanol was taken, to which 24 mg of DPPH and dissolved. Different dilutions of the test compound, ranging from 62.50 to 1000 μg mL^{-1} were prepared. One mL of DPPH solution was added to 1 mL of test sample dilution and subsequently incubated in dark place for 30 min at 23 °C. Subsequent to incubation, absorbance values were recorded at 517 nm via UV–visible spectrophotometer. The positive control was ascorbic acid, whereas the negative control was DPPH solution without test sample. Percent scavenging of test compounds was determined via formula;

$$\%FRSA = \left(\frac{Ab_C - Ab_S}{Ab_C} \right) \times 100$$

In vivo diabetic studies

Animals and approval of ethical committee

BALB/c albino mice were utilized for the anti-diabetic study. Animals were acquired from NIH Pakistan and looked after in the animal house of the University of Malakand. Animals were maintained under normal day/night cycle (12 h light and 12 h dark) and provided enough food and ad libitum. The procedure and project were approved by research ethics committee at the Department of Pharmacy, University of Malakand. All animals procedure and handling were performed following the Commission on life sciences, National research council 1996 (Council) (NRC 1996).

Acute toxicity test

To analyze the toxicological effects of our test sample, albino mice were classified into different groups (n = 5) and were administered i/p dose of 200–2000 mg kg^{-1} of our test compound. Animals were closed observed for one week for the appearance of any symptoms of toxicity including lethality or any aberrant behavior (Ayaz et al. 2017; Mir et al. 2019).

Induction of diabetes

For diabetes induction, mice were kept in fasting for 8–12 h and ten percent alloxan-monohydrate (150 mg kg^{-1}) was administered intraperitoneally (I/P). Normal saline (NS) was given to control group. Following inducing of DM, blood glucose level was calibrated with glucose meter and only diabetic animals for further proceedings were proceeded (Hussain et al. 2019).

Experiment design

Mice were divided randomly into 4 groups and each group constituted of 5 mice. The concentration of glucose in blood was observed at 0th, 1st, 4th, 7th, 11th, 14th, and 21st days of treatment.

> Group I: Diabetic group was given alloxan and Tween 80 (I/P).
> Group II: Control nondiabetic group was given normal saline only (I/P).
> Group III: Treatment group was given glibenclamide (dose μg kg^{-1}) PO.
> Group IV: Treatment group received test compound (dose μg kg^{-1}) (I/P).

Oral glucose tolerance test (OGTT)

To evaluate the animal's glucose tolerance capacity after oral glucose administration, animals of both groups including normal control and disease control were kept on fasting overnight. Subsequently, 2 mg/kg oral glucose was administered to each animal. Blood glucose was monitored at different times from (0 to120 min) after administration of glucose (Mahnashi et al. 2022a).

Drugs administration and assessment of blood glucose level

Animals were distributed in four groups. Group 1 was administered Alloxan at 150 mg kg^{-1} dose and tween 80 and acted as disease control group. This group was untreated and was kept for comparison with the treated groups. Group 2 was placebo group which was maintained on normal diet for comparison, Group 3 was disease group administered with standard drug glibenclamide at 5 mg/kg dose daily for 21 days. Further, group 4 was disease group which was maintained on 30 mg/kg dose of our test compound. Blood glucose levels were monitored three times a day using glucometer (Viva check Inox Laboratories Wilmington USA) and were observed for 21 days (Shaheen et al. 2016).

Mohamed *et al. AMB Express* (2023) 13:24

Page 6 of 14

Blood biochemistry analysis

Animals were euthanized at the end of experiments, via halothane anesthesia following standard procedure and samples of blood from lateral tail were collected for further analysis. Blood tests including cholesterol level, triglycerides, LDL, HDL, and total lipids were analyzed via techno 786 semi-automated biochemistry analyzer. Colorimetric enzymatic test using glycerol-3-phosphate-oxidase (gpo) and Chod-Pap enzymatic photometric tests were employed for the analysis (Pundir and Aggarwal 2017).

Statistical analysis

Experimental procedures were performed three times and the results are reported as Mean ± SEM. One way ANOVA and multiple comparison DUNNETT's test was used for the statistical comparison of the treatment and control groups using Graph Pad Prism version 5.

Estimation of median inhibitory concentrations

The dose–response curve was used to calculate the Median inhibitory concentrations (IC_{50}) using using Graph Pad Prism version 5.

Results

Characterization

The room temperature physico-chemical attributes of the HT-Er_2O_3 NPs were studied using XRD, FTIR spectroscopy, Reflectance spectroscopy as indicated in the inset Fig. 2(A–D). The X-ray diffraction pattern revealed sharp peaks for 2θ position at 29°, 33°, 48° and 57.9° which can be assigned to the crystallographic reflections of (222), (400), (440) and (622). These results are perfectly in
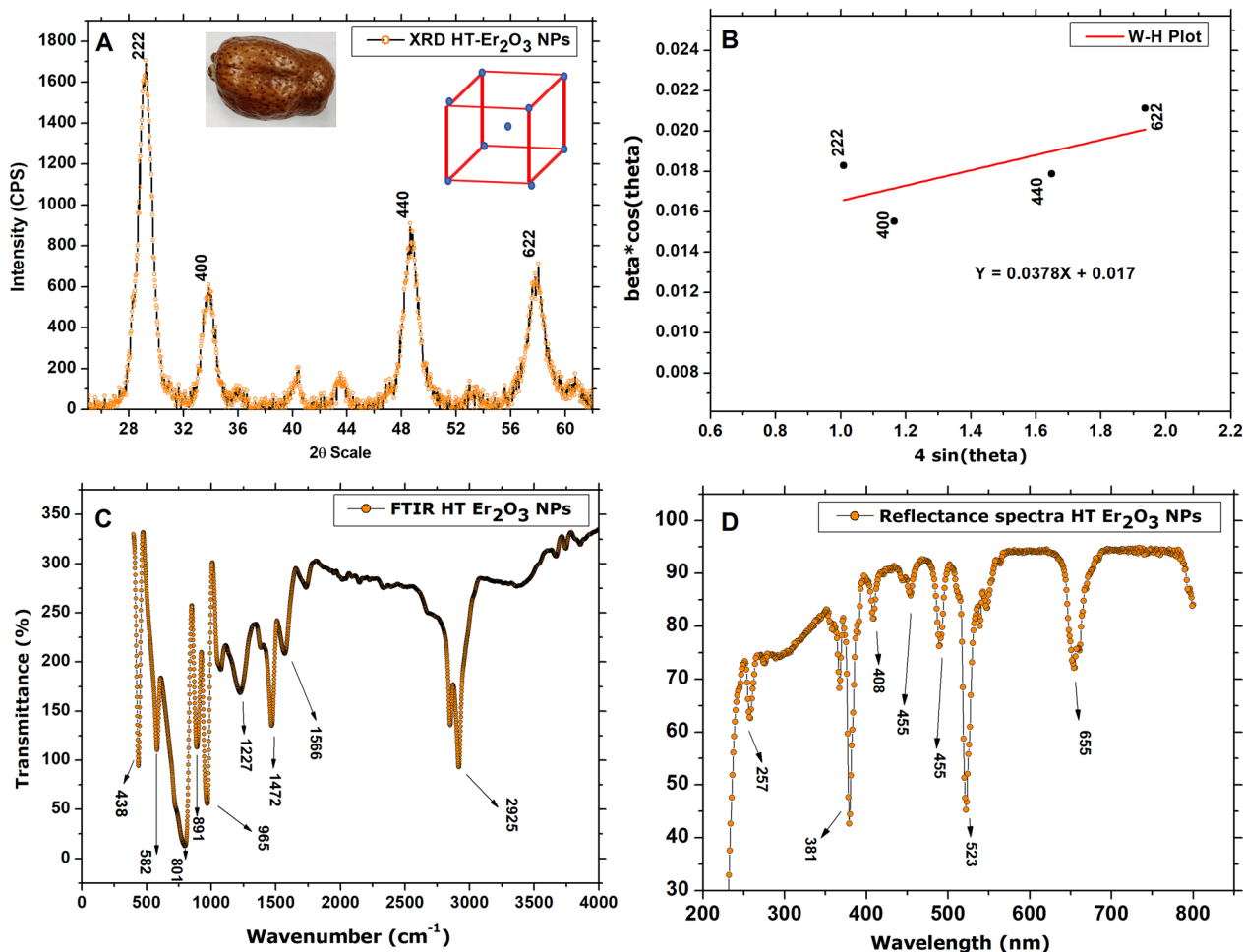

Fig. 2 Room temperature physical properties of the HT-Er_2O_3 NPs; (**A**) X-ray diffraction pattern; (**B**) Williamson Hall Plot analysis of the HT-Er_2O_3 NPs (From the linear fit, data is extracted to calculate the strain from the slop and crystallite size from the y-intercept); (**C**) FTIR spectra of HT-Er_2O_3 NPs; (**D**) Reflectance spectra of HT-Er_2O_3 NPs

Mohamed *et al. AMB Express* (2023) 13:24

Page 7 of 14

Table 1 Grain or crystallite size of the HT-Er$_2$O$_3$ NPs

2θ	hkl	FWHM	Grain or crystallite size (nm)
222	222	1.16335	7.37
400	400	1.06846	8.13
440	440	1.1669	7.79
622	622	1.35403	6.98
Average grain or crystallite size		D = 7.56 nm	
Dislocation density		$\delta = 1/D^2 = 0.0174$ nm^{-2}	
Grain or crystallite size using Williamson-Hall method		11 nm	
Dislocation density		$\delta = 1/D^2 = 0.008$ nm^{-2}	
Strain (ε)		0.0378	

accord with the JCPDS card no. 00-043-1007, that corresponds to the Er$_2$O$_3$ with body centered cubic crystal lattice. The average crystallite or grain size of HT-Er$_2$O$_3$ NPs calculated according to the Debye Scherrer approximation (Eq. 1) was found to be ~ 7.56 nm. Obtained calculations are shown in Table 1. The crystallite or grain size calculated from the W–H plot method was found to be 11 nm using (Eq. 2). The results are indicated in Fig. 2B. The dislocation density was calculated as 0.

Figure 2C indicates the FTIR spectra of the HT-Er$_2$O$_3$ NPs, for evaluation of their vibrational properties to understand their structural and functional nature. The FTIR spectra reveals typical metal oxide vibrations in the fingerprint region. Peaks positioned at ~ 438 cm^{-1}

and 582 cm^{-1} can be assigned to the Er-O and Er-O-Er, that confirms the synthesis of erbium oxide nanoparticles. The vibrations between 800 cm^{-1} and 3000 cm^{-1} can be ascribed to the specific surface activities, attached functional groups, surface adsorbed moisture or other phenolic compounds. The IR bands can be assigned to different functional groups like ~ 801 cm^{-1} (amine group), 891 cm^{-1} (C–H vibration from aromatic compounds), 965 cm^{-1} (O–H vibration), 1227 cm^{-1} (C–O vibration), 1472 cm^{-1} (C–H bending mode of alkanes), 1566 cm^{-1} (C–C stretching of aromatic compounds), 2925 cm^{-1} (C–H stretching of alkanes). Figure 2D indicates reflectance spectra which was used to derive the optical bandgap (5.25 eV) using Kubelka–Munk function (K–M), i.e., by plotting $(F(R)h\nu)^2$ on y-axis against hv on x-axis, as indicated in Fig. 3A. The K-M function can be determined by using the following formula;

$$FR = {(1 - R)^2}\big/{2R} \qquad (4)$$

here, "R" is the reflectance, "FR" is the Kubelka–Munk function.

Raman spectrum revealed (100 cm^{-1}–1400 cm^{-1}) revealed seven major peaks centered at ~ 261 cm^{-1}, 562 cm^{-1}, 647 cm^{-1}, 741 cm^{-1}, 832 cm^{-1}, 978 cm^{-1} and 1071 cm^{-1} as indicated in Fig. 3B. Between 240 and 300 cm^{-1} there are an isolated group of three lines (2 A$_g$ + B$_g$) is observed to which no Raman line corresponds in A -type spectra. These bands are assigned to the (2 A$_g$ + B$_g$) modes deriving from (A$_{2u}$ + E$_u$) infrared
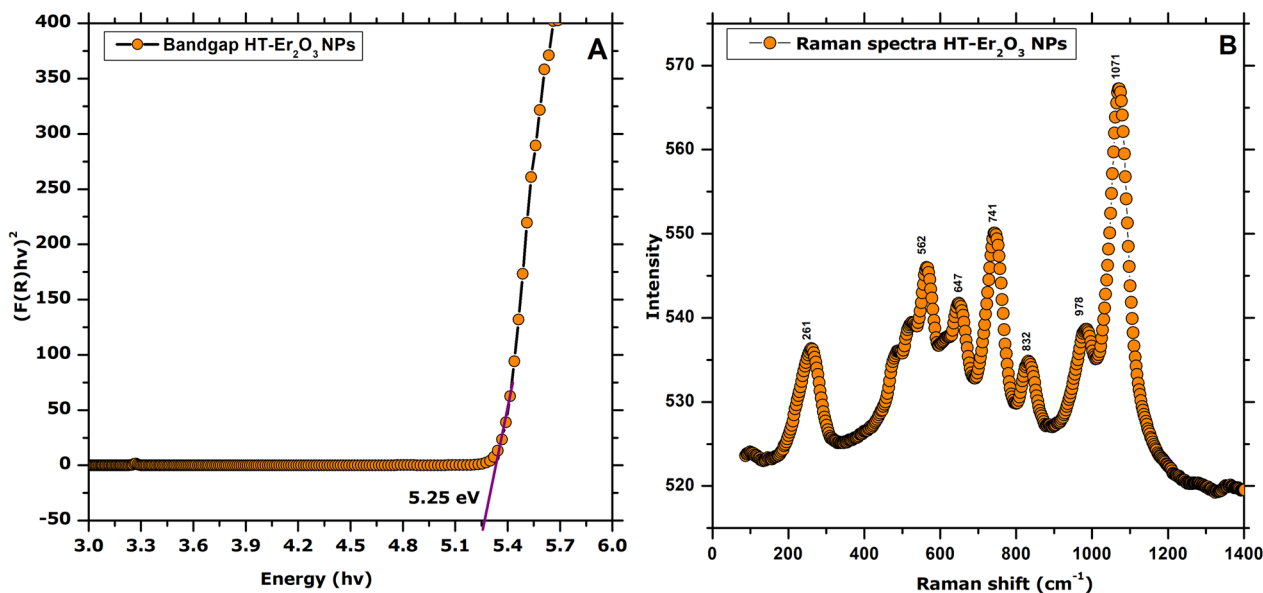

Fig. 3 Bandgap calculation and Raman Spectra (**A**) Plots of $(F(R)h\nu)^2$ versus the photon energy (hv) after applying K–M function for calculated the optical bandgap; (**B**) Raman spectra of HT-Er$_2$O$_3$ NPs
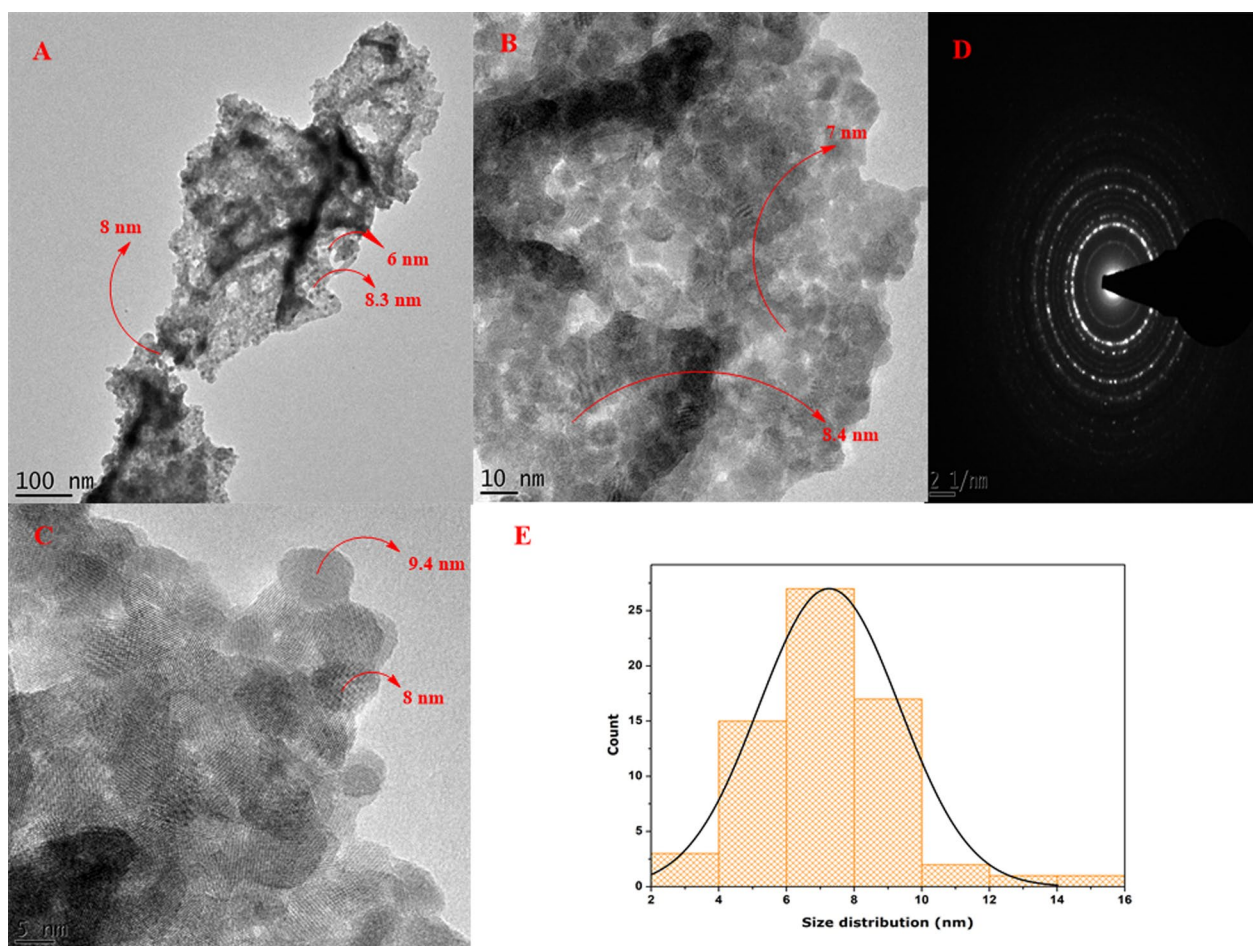
Mohamed *et al. AMB Express* (2023) 13:24

Page 8 of 14

Fig. 4 High resolution transmission electron microscopy of HT-Er$_2$O$_3$ NPs; (**A–C**): HR-TEM images at different magnifications; (**D**): Selected Area Electron Diffraction pattern of HT-Er$_2$O$_3$ NPs; (**E**) Particle size distribution of the HT-Er$_2$O$_3$ NPs

active modes and involving Er-O bonds. Between 350 and 600 cm^{-1}, the last group of Raman lines would correspond to the splitting of the A$_{1g}$ + E$_g$ stretching vibrations the frequencies of which are very close in the cubic phase. Peaks between 800 and 1200 cm^{-1} are assigned to different functional groups coming from the *H. thebaica* extract which confirmed as well with FTIR.

HR-TEM images at different magnifications were used to identify shape and obtain the size distribution as indicated in the inset Fig. 4A–C. The nanoparticles appeared to be cuboidal and quasi-spherical (Figure A–C), whereas, the size distribution results histogram revealed that most of the nanoparticles were around the range of 6–8 nm (Fig. 4E). The selected area electron diffraction pattern as indicated in Fig. 4D, revealed spotty rings which reaffirmed that the HT-Er$_2$O$_3$ NPs are of highly crystalline nature.
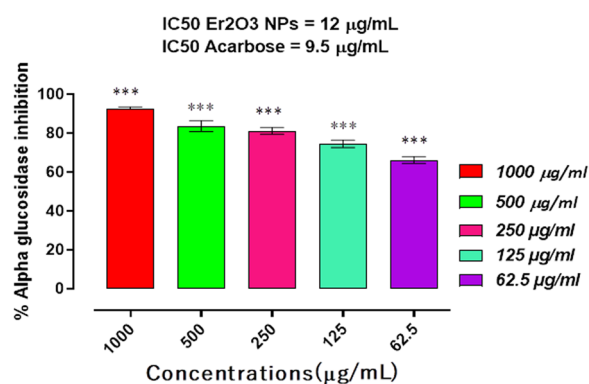

Fig. 5 Results of Er$_2$O$_3$ NPS inhibitory potentials against α-glucosidase enzyme. Results were presented as mean ± SEM of three independent experimental observations. *** represents p value < 0.001 when compared with placebo group. Acarbose was used as positive control
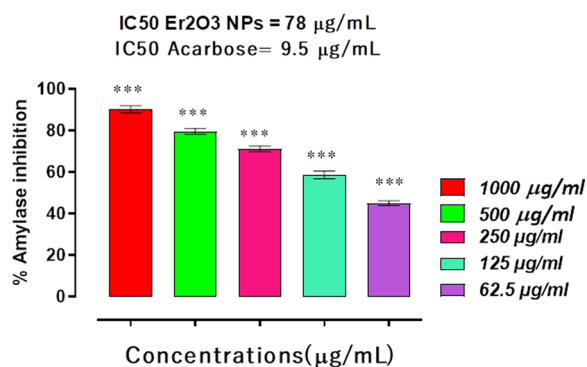
Fig. 6 Results of Er_2O_3 NPS inhibitory potentials against α-amylase enzyme.Results were presented as mean ± SEM of three independent experimental observations. *** represents p value < 0.001 when compared with placebo group

α-glucosidase inhibition

The synthetic HT-Er_2O_3 NPs exhibited concentration-dependent inhibitory potentials against alpha-glucosidase enzyme. Results of the standard drug acarbose were comparable as shown in Fig. 5. The percent inhibition against α-glucosidase by HT-Er_2O_3 NPs at the different test concentrations in the range of (1000 μg mL^{-1} to 62.5 μg mL^{-1}) were 92.30, 83.60, 81.15, 74.43 and 66.13 percent respectively with IC$_{50}$ value of 12 μg mL^{-1}. The positive control, acarbose displayed the IC$_{50}$ values of 9.5 μg mL^{-1}.

HT-Er_2O_3 NPs inhibit α-amylase enzyme

Again HT-Er_2O_3 NPs exhibited considerable inhibition against α-amylase enzyme in comparison to control drug as shown in Fig. 6. The observed percent inhibitions by HT-Er_2O_3 NPs were 90.30, 79.63, 71.20, 58.67, and 45.00 at concentrations of (1000 μg mL^{-1} to 62.5 μg mL^{-1}), respectively with IC$_{50}$ value of 78 μg mL^{-1}. The IC$_{50}$ value of positive control, acarbose was 9.5 μg mL^{-1}.
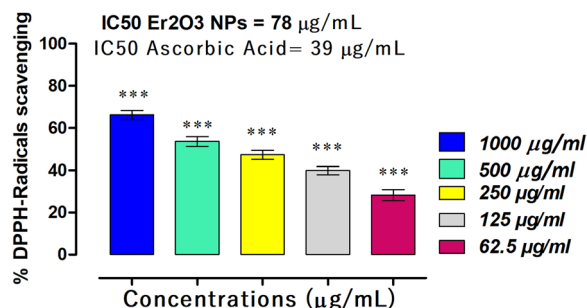

Fig. 7 Results of Er_2O_3 NPS DPPH radical scavenging potential. *** represents p value < 0.001 when compared with positive control group

HT-Er_2O_3 NPs scavenge DPPH radicals

In this assay, the synthesized HT-Er_2O_3 NPs exhibited high percent activity against DPPH free radicals with concentration dependent manner (Fig. 7). The synthesized HT-Er_2O_3 NPs showed 66.25, 53.63, 47.23, 39.82 and 28.31 percent scavenging at the concentrations of (1000 μg mL^{-1} to 62.5 μg mL^{-1}) respectively with IC$_{50}$ of 78 μg mL^{-1}. The % DPPH scavenging of HT-Er_2O_3 NPs was compared with Ascorbic acid (positive control), whose IC$_{50}$ value was 39 μg mL^{-1}.

Acute toxicity test

In acute toxicity study, no animals' lethality was observed for one week. Further, no cyanosis, spontaneous activity, tail pinch, aggressiveness, convulsions or bizarre behavior was observed during the course of study. So, our sample was observed to be safe at the tested concentrations, though its chronic effects on individual organs need further detailed studies.

OGTT results

After induction of diabetes and administration of oral dose of glucose the blood glucose was 370.66 μg dL^{-1} at 0 time, 411.00 μg dL^{-1} after 30 min, 449.33 μg dL^{-1} at 60 min and 552.66 μg dL^{-1} after 120 min. Results of the assay is indicated in Fig. 8.

HT-Er_2O_3 NPs exhibited considerable anti-hyperglycemic effects

Results of various treatments on blood glucose level of animals is summarized in Table 2. Briefly, in disease group (group 1) the blood glucose level was observed to be elevated persistently 567.00 ± 3.46 mg dL^{-1} on day 0, till 389.33 ± 4.50 mg dL^{-1} on day 21. Blood glucose level of saline treated group (group 2) was within the range throughout the study. Though it was little elevated 115.33 ± 7.86*** mg dL^{-1} l at the start of experiment but then stabilized and on day 21 it was 93.50 ± 1.60*** mg dL^{-1}. Positive control, group (group
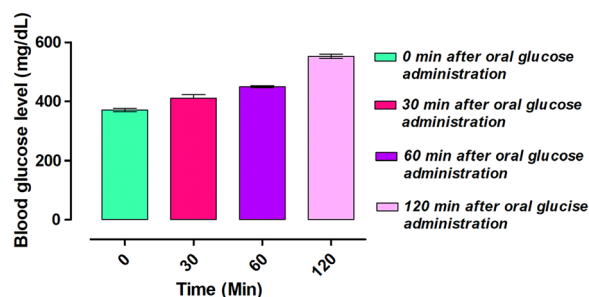

Fig. 8 Results of the oral glucose tolerance test (OGTT)

Mohamed *et al. AMB Express*   (2023) 13:24

Page 10 of 14

Table 2 Effect of various treatments on blood glucose levels of diabetic animal

S. No.	Groups	Dose mg kg^{-1}	Blood glucose level (GL) (mg dL^{-1})						
			Day 0	Day 1	Day 4	Day 7	Day 11	Day 14	Day 21
Group1	After Alloxan + Tween 80	150	567.00 ± 3.46	507.00 ± 5.77	522.66 ± 3.75	500.66 ± 4.33	469.66 ± 2.60	454.33 ± 2.96	389.33 ± 4.50
Group2	Normal control saline	0.35	115.33 ± 7.86***	121.00 ± 3.51***	116.50 ± 2.66***	108.33 ± 2.89***	103.00 ± 4.50***	97.00 ± 1.50***	93.50 ± 1.60***
Group3	Glibenclamide	05	376.66 ± 1.20***	351.33 ± 5.20***	341.00 ± 3.66***	361.50 ± 2.50***	301.38 ± 2.33***	279.88 ± 3.80***	235.33 ± 2.33***
Group4	HT-Er$_2$O$_3$ NPs	30	503.66 ± 5.92***	458.66 ± 2.02***	375.00 ± 3.09***	310.66 ± 2.33***	298.00 ± 4.04***	205.33 ± 2.60***	185.66 ± 2.60***

*** $p < 0.001$ at 95% confidence interval

3) maintained the blood glucose level of diabetic animals
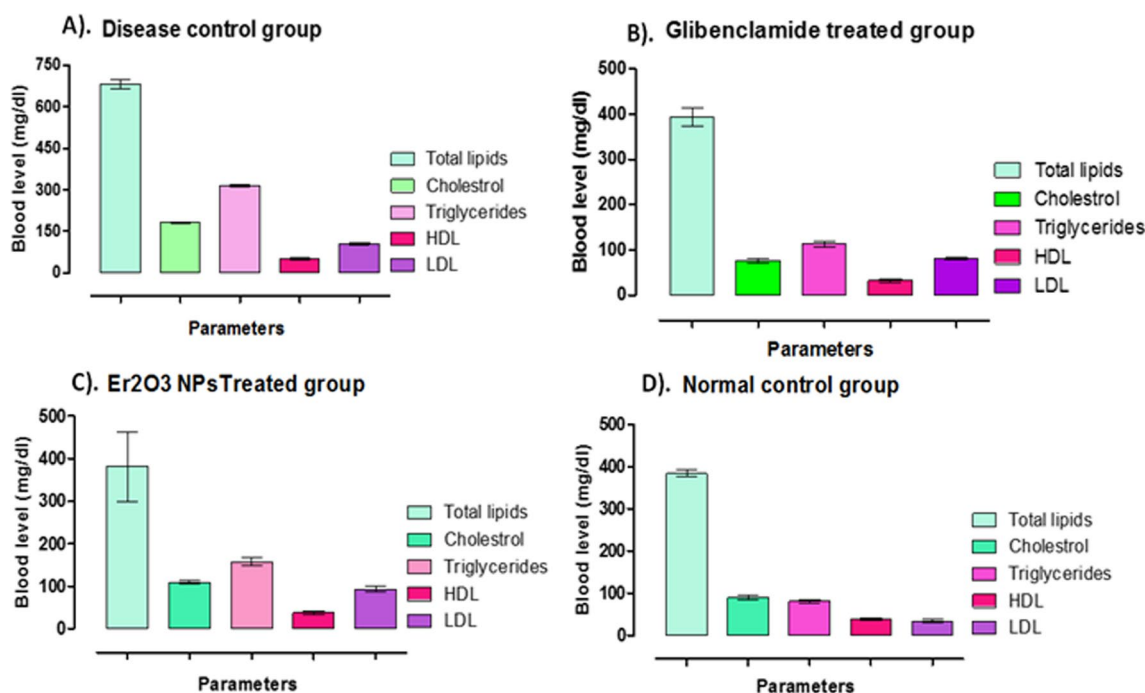
Biochemical analysis of blood

Fig. 9 Effect of Er$_2$O$_3$ NPs therapy on serum lipids including total lipids, cholesterol, triglycerides, HDL and LDL. (**A**): Disease group; (**B**): Positive control group, (**C**): Er$_2$O$_3$ NPs treated group; (**D**): Normal group

in an average range of (376.66 ± 1.20*** mg dL^{-1} on day 0, 351.33 ± 5.20*** mg dL^{-1} on day 1, 341.00 ± 3.66*** mg dL^{-1} on day 4, 301.38 ± 2.33*** mg dL^{-1} on day 11, 279.88 ± 3.80*** mg dL^{-1} on day 14 and 235.33 ± 2.33*** mg dL^{-1} on day 21. Overall glibenclamide was unable to control hyperglycemia in diabetic animals. Our tested compound HT-Er$_2$O$_3$ NPs have exhibited better control over blood glucose level of the diabetic animals (503.66 ± 5.92*** on day 0 and 185.66 ± 2.60*** on day 21).

Results of the biochemical analysis of blood is summarized in the inset Fig. 9A–D. In disease group, average total lipids were 682.33 µg dL^{-1}, cholesterol level was 180.66 µg dL^{-1}, triglycerides were 315.00 µg dL^{-1}, HDL was 51.33 and LDL was 105 mg/dl respectively (Fig. 9A). Treatment with HT-Er$_2$O$_3$ NPs have normal blood parameters i.e. total lipids, cholesterol, triglycerides, HDL and LDL after 21 days as observed in Fig. 9C. The blood glucose level was at comparatively low level in the positive control group indicating reduction in

Mohamed *et al. AMB Express*   (2023) 13:24

Page 11 of 14

the hyperglycemia mediated changes in the blood total lipids, triglycerides, cholesterol, HDL and LDL levels (Figure C).

Discussion

Biological synthesis of the metal NPs provides an eco-friendly and one-step process for the synthesis of novel metal nanoparticles. Previously, we have demonstrated synthesis of Fe_2O_3 (Mohamed et al. 2020b), CeO_2 (Mohamed et al. 2020a), $Cr2O_3$ (Mohamed et al. 2020), $BiVO_4$ (Mohamed et al. 2019b), ZnO (Mohamed et al. 2020c), CuO (Mohamed et al. 2021) and Ag nanoparticles (Mohamed et al. 2019a) using the fruit material of *Hyphaene thebaica* fruit material. To date, the exact mechanism of bioreduction leading to the synthesis of metal nanoparticles is not well explored because of the heterogeneity of the plant extracts (Dauthal and Mukhopadhyay 2016). Plant phytochemicals possess different chemical and physical properties including metal ion reduction and stabilization (Abomuti et al. 2021). The generally proposed mechanism includes a simple bioreduction and stabilization process which is mediated by the phytochemical constituents in the plant extracts. Phytochemicals plays a dual role, thereby, at first reduces the metal salt in to ions, in this case reducing the erbium nitrate, followed by stabilization through the capping or coating agents found in the fruit extracts of the *Hyphaene thebaica.* The intricate nature and phytochemistry of the plant extracts makes it difficult to specify a particular class of specific biomolecules in metal reduction, stabilization and morphological control of NPs (Huo et al. 2022).

Here, the green synthesis of nano-erbia is reported for the first time in the literature. Medicinal plants like *H. thebaica* have a rich phytochemistry and includes compounds like vanillic acid, cinnamic acid, sinapic acid, caffeic acid, chlorogenic acid, epicatechin, hesperetin, naringin, glycosides, quercetin, rutin, tannins, saponins etc. Such phenolic and flavonoid compounds have the ability to execute redox reactions and subsequently stabilize the nanoparticles (El-Beltagi et al. 2018; Islam et al. 2022; Jadoun et al. 2021; Jeevanandam et al. 2022; Karatoprak et al. 2017). Previous studies have indicated that the phenolic compounds possess strong reducing ability and hence most likely agents for catalyzing the bioreduction as compared to other macromolecules in plant extracts like carbohydrates and proteins (Huo et al. 2022).

X-rays diffraction pattern was found to be consistent with the previously published literature (Munawar et al. 2020; Wang et al. 2018b). Similarly, the FTIR peak at ~ 438 (Er-O) cm^{-1} and ~ 582 cm^{-1} (Er-O-Er) are in agreement with reported literature (Azad and Maqsood 2014). The FTIR signature indicated that different phytochemicals available in the pristine aqueous fruit extracts were responsible for the reduction and capping process and eventually led to the synthesis of stable nanoparticles (Khan et al. 2013). The optical bandgap of the HT-Er_2O_3 NPs was calculated 5.25 eV by applying the K–M function which is correlates with values reported in the literature (Kamineni et al. 2012; Kao et al. 2012). The Raman vibrations corelates with the previous studies (Joya et al. 2019).

Diabetes mellitus (DM) is a disorder of metabolism of glucose that encompasses raised levels of blood glucose and other complications like neuropathy, retinopathy, nephropathy, and micro and macrovascular complications (Arky 1982). Defects in the production, secretion and action of insulin are responsible for hyperglycemia (Booth et al. 2016). DM affects about five percent population worldwide and its occurrence is increasing at an alarming rate, and is also associated with number of other diseases (Rahim et al. 2019). There are about 450 million peoples around the world which are effected by DM and the numbers are expected to grow up to 690 million by 2044 (Cho et al. 2018). Type 1 (T1DM) and Type 2 (T2DM) are the important kinds of DM. (Del Prete et al. 1977; Himsworth and Kerr 1939). Type 1 diabetes is an immune-associated, destruction of insulin-producing pancreatic β cells (Atkinson et al. 2011). Type 1 diabetes treatment includes the use of insulin and its analogues. T2DM can be managed by controlling diet, obesity and with anti-diabetic drugs (Ohlson et al. 1985). In the development of antidiabetic therapeutic agents, α–amylase and α–glucosidase inhibitors are the vital targets. These enzymes breakdown polysaccharides (starch) to glucose and the inhibition of these enzymes play an important role to reduce glucose absorption in the intestine (Gin and Rigalleau 2000). There are several therapeutic approaches used for the treatment of diabetes, like lowering postprandial hyperglycemia by hydrolyzing α-amylase and α-glucosidase enzyme inhibition (Wang et al. 2018a). Anti-diabetic drugs as enzyme inhibitors like acarbose, voglibose, and miglitol were utilized for years to treat diabetes (Chaudhury et al. 2017).

Plants contains numerous secondary metabolites exhibiting different properties including the metal ion reduction and stabilization. The interaction of plants with metals as a natural process and have got the attention of many scientists to utilize the secondary metabolites of plants as a reducing and stabilizing agent (Javed et al. 2021). The biosynthesis of metal NPs utilizing medicinal plants serve as alternative to utilizing hazardous chemical and physical synthetic techniques (Anand et al. 2017). We for the first-time synthesized HT-Er_2O_3 NPs by using plant extracts as reducing and stabilizing

Mohamed *et al. AMB Express*   (2023) 13:24

Page 12 of 14

agents. The prepared nanoparticles were extensively characterized in their in-vitro and in-vivo assays were performed for determination of its antioxidant and anti-diabetic potential.

The synthetic HT-Er_2O_3 NPs exhibited concentration dependent inhibition against α-glucosidase and the percent inhibition at the concentrations of 1000, 500, 250, 125 and 62.5 μg mL^{-1} was 92.30, 83.60, 81.15, 74.43 and 66.13 percent respectively with IC$_{50}$ value of 12 μg mL^{-1}. In α-amylase inhibition assay, HT-Er_2O_3 NPs showed 90.30, 79.63, 71.20, 58.67, and 45.00 percent inhibition at concentrations of 1000, 500, 250, 125, and 62.50 μg mL^{-1}, respectively with IC$_{50}$ value of 78 μg mL^{-1}. In DPPH free radical scavenging assay, the synthesized HT-Er_2O_3 NPs showed 66.25, 53.63, 47.23, 39.82 and 28.31 percent inhibition at the concentrations of 1000, 500, 250, 125 and 62.5 μg mL^{-1} respectively with IC$_{50}$ of 78 μg mL^{-1} (Fig. 1). Animal studies revealed that our tested sample are safe at higher doses and was effective in lowering post-prandial hyperglycemia. As summarized in Table 2, our tested compound HT-Er_2O_3 NPs have exhibited better control over blood glucose level of the diabetic animals (503.66 ± 5.92*** on day 0 and 185.66 ± 2.60*** on day 21 as compared to standard drug glibenclamide. Er_2O_3 NPs therapy for 21 day has normalized hyperlipidemia. Thus in-vitro enzyme inhibition coupled with anti-radical properties and in-vivo anti-hyperglycemic and anti-hyperlipidemic potentials make it a potential candidate for further detailed studies.

Our findings suggest that our synthetic HT-Er_2O_3 NPs have considerable antidiabetic potential via α–glucosidase and α–amylase enzymes inhibition which are the potential targets in the development of antidiabetic drugs. Considerable in-vivo anti-hyperglycemic and anti-hyperlipidemic potentials were observed for HT-Er_2O_3 NPs and thus it warrants further detailed studies.

Availability of data and materials
All the data generated as a result of this current research has been included in the manuscript.

Declarations

Ethics approval and consent to participate
This study does not include any human participants. The animal related procedures have been approved by the Departmental Research Ethics Committee of the Department of Pharmacy, University of Malakand, vide letter no. DREC/Pharm/2022–05.

Consent for publications
All the contributing authors have reviewed the manuscript and have given their consent for publications.

Competing interests
Authors declares that they have no competing interests.

References

Abdulazeez M, Bashir A, Adoyi B, Mustapha A, Kurfi B, Usman A, Bala R (2019) Antioxidant, hypolipidemic and angiotensin converting enzyme inhibitory effects of flavonoid-rich fraction of Hyphaene thebaica (Doum Palm) fruits on fat-fed obese wistar rats. Asian J Res Biochem:1–11

Abomuti MA, Danish EY, Firoz A, Hasan N, Malik MA (2021) Green synthesis of zinc oxide nanoparticles using salvia officinalis leaf extract and their photocatalytic and antifungal activities. Biology 10(11):1075

Acikgoz A, Ceyhan G, Aktas B, Yalcin S, Demircan G (2021) Luminescent, structural and mechanical properties of erbium oxide doped natural obsidian glasses. J Non-Cryst Solids 572:121104

Anand K, Tiloke C, Naidoo P, Chuturgoon A (2017) Phytonanotherapy for management of diabetes using green synthesis nanoparticles. J Photochem Photobiol, B 173:626–639

Arky R (1982) Clinical correlates of metabolic derangements of diabetes mellitus. In: Kozak GP (ed) Complications of Diabetes mellitus. Saunders WB, Philadelphia

Atkinson MA, Bluestone JA, Eisenbarth GS, Hebrok M, Herold KC, Accili D, Pietropaolo M, Arvan PR, Von Herrath M, Markel DSJD (2011) How does type 1 diabetes develop?: the notion of homicide or β-cell suicide revisited. 60(5):1370–1379

Ayaz M, Junaid M, Ullah F, Subhan F, Sadiq A, Ali G, Ovais M, Shahid M, Ahmad A, Wadood A (2017) Anti-Alzheimer's studies on β-sitosterol isolated from polygonum hydropiper L. Front Pharmacol 8:697

Azad F, Maqsood A (2014) Fabrication, structural characterization, dielectric and electrical parameters of the synthesized nano-crystalline erbium oxide. Electron Mater Lett 10(3):557–563

Bindu P, Thomas S (2014) Estimation of lattice strain in ZnO nanoparticles: X-ray peak profile analysis. J Theor Appl Phys 8(4):123–134

Booth G, Lipscombe L, Butalia S, Dasgupta K, Eurich D, Goldenberg R, Khan N, MacCallum L, Shah B, Simpson S (2016) Pharmacologic management of type 2 diabetes: 2016 interim update. Can J Diabetes 40(6):484–486

Chaudhury A, Duvoor C, Reddy Dendi VS, Kraleti S, Chada A, Ravilla R, Marco A, Shekhawat NS, Montales MT, Kuriakose K (2017) Clinical review of antidiabetic drugs: implications for type 2 diabetes mellitus management. Front Endocrinol 8:6

Chittaranjan Patra IA, Ayaz M, Khalil AT, Mukherjee S, Ovais M (2021) Biogenic Nanoparticles for Cancer Theranostics, 1st edn. Elsevier, Amsterdam

Cho N, Shaw J, Karuranga S, Huang Yd, da Rocha FJ, Ohlrogge A, Malanda B (2018) IDF diabetes atlas: global estimates of diabetes prevalence for 2017 and projections for 2045. Diabetes Res Clin Pract 138:271–281

Mohamed *et al. AMB Express*   (2023) 13:24

Page 13 of 14

Dauthal P, Mukhopadhyay M (2016) Noble metal nanoparticles: plant-mediated synthesis, mechanistic aspects of synthesis, and applications. Ind Eng Chem Res 55(36):9557–9577

Dědková K, Kuzníková Ľ, Pavelek L, Matějová K, Kupková J, Barabaszová KČ, Váňa R, Burda J, Vlček J, Cvejn D (2017) Daylight induced antibacterial activity of gadolinium oxide, samarium oxide and erbium oxide nanoparticles and their aquatic toxicity. Mater Chem Phys 197:226–235

Del Prete GF, Betterle C, Padovan D, Erle G, Toffolo A, Bersani G (1977) Incidence and significance of islet-cell autoantibodies in different types of diabetes mellitus. Diabetes 26(10):909–915

Dhanasekaran S, Perumal P, Palayan M (2015) In-vitro Screening for acetylcholinesterase enzyme inhibition potential and antioxidant activity of extracts of Ipomoea aquatica Forsk: therapeutic lead for Alzheimer's disease. J Appl Pharm Sci 5:012–016

Diallo A, Mothudi BM, Manikandan E, Maaza M (2016) Luminescent Eu2O3 nanocrystals by Aspalathus linearis' extract: structural and optical properties. J Nanophotonics 10(2):026010

El-Beltagi HS, Mohamed HI, Yousef HN, Fawzi EM (2018) Biological activities of the doum palm (Hyphaene thebaica L) extract and its bioactive components. Antioxidants in Foods and its Applications 49

Gin H, Rigalleau V (2000) Post-prandial hyperglycemia post-prandial hyperglycemia and diabetes. Diabetes Metab 26(4):265–272

Guler Ö, Guler SH, Yo F, Aydin H, Aydin C, El-Tantawy F, Duraia E-SM, Fouda A (2015) Electrical and optical properties of carbon nanotube hybrid zinc oxide nanocomposites prepared by ball mill technique. Fullerenes Nanotubes Carbon Nanostruct 23(10):865–869

Himsworth H, Kerr R (1939) Insulin-sensitive and insulin-insensitive types of diabetes mellitus. Clin Sci 4:119–152

Huo C, Hao Z, Yuan C, Chen Y, Liu J (2022) Probing the phytosynthesis mechanism of gold and silver nanoparticles by sequential separation of plant extract and molecular characterization with ultra-high-resolution mass spectrometry. ACS Sustain Chem Eng 10(12):3829–3838

Hussain F, Khan Z, Jan MS, Ahmad S, Ahmad A, Rashid U, Ullah F, Ayaz M, Sadiq A (2019) Synthesis, in-vitro α-glucosidase inhibition, antioxidant, in-vivo antidiabetic and molecular docking studies of pyrrolidine-2, 5-dione and thiazolidine-2, 4-dione derivatives. Bioorg Chem 91:103128

Islam F, Saeed F, Afzaal M, Hussain M, Al Jbawi E, Armghan Khalid M, Asif Khan M (2022) Nutritional and functional properties of Hyphaene thebaica L flour: a critical treatise and review. Int J Food Prop 25(1):1234–1245

Jadoun S, Arif R, Jangid NK, Meena RK (2021) Green synthesis of nanoparticles using plant extracts: a review. Environ Chem Lett 19(1):355–374

Javed B, Ikram M, Farooq F, Sultana T, Z-u-R M, Raja NI (2021) Biogenesis of silver nanoparticles to treat cancer, diabetes, and microbial infections: a mechanistic overview. Appl Microbiol Biotechnol 105(6):2261–2275

Jeevanandam J, Kiew SF, Boakye-Ansah S, Lau SY, Barhoum A, Danquah MK, Rodrigues J (2022) Green approaches for the synthesis of metal and metal oxide nanoparticles using microbial and plant extracts. Nanoscale 14(7):2534–2571

Joya M, Alfonso J, Moreno L (2019) Photoluminescence and Raman studies of α-MoO3 doped with erbium and neodymium. Curr Sci India 116:1690–1695

Kamal Z, Ullah F, Ayaz M, Sadiq A, Ahmad S, Zeb A, Hussain A, Imran M (2015) Anticholinesterase and antioxidant investigations of crude extracts, subsequent fractions, saponins and flavonoids of atriplex laciniata L potential effectiveness in Alzheimer's and other neurological disorders. Biol Res 48(1):1–11

Kamineni HS, Kamineni VK, Moore RL, Gallis S, Diebold AC, Huang M, Kaloyeros AE (2012) Optical and structural characterization of thermal oxidation effects of erbium thin films deposited by electron beam on silicon. J Appl Phys 111(1):013104

Kao C-H, Chen H, Pan YT, Chiu JS, Lu T-C (2012) The characteristics of the high-K Er2O3 (erbium oxide) dielectrics deposited on polycrystalline silicon. Solid State Commun 152(6):504–508

Karatoprak GŞ, Aydin G, Altinsoy B, Altinkaynak C, Koşar M, Ocsoy I (2017) The effect of pelargonium endlicherianum Fenzl root extracts on formation of nanoparticles and their antimicrobial activities. Enzyme Microb Technol 97:21–26

Khalil AT, Khan MD, Razzaque S, Afridi S, Ullah I, Iqbal J, Tasneem S, Shah A, Shinwari ZK, Revaprasadu N (2021b) Single precursor-based synthesis of transition metal sulfide nanoparticles and evaluation of their antimicrobial, antioxidant and cytotoxic potentials. Appl Nanosci 11(9):2489–2502

Khalil NA, Motaal AA, Meselhy K (2018) Renin and angiotensin converting enzyme inhibition of standardized bioactive fractions of Hyphaene thebaica L mart growing in Egypt. Pharmacognosy Journal 10(4)

Khalil AT, Iqbal J, Shah A, Haque MZ, Khan I, Ayaz M, Ahmad I, Tasneem S, Shah H (2021a) The bio–nano interface as an emerging trend in assembling multi-functional metal nanoparticles

Khan M, Khan M, Adil SF, Tahir MN, Tremel W, Alkhathlan HZ, Al-Warthan A, Siddiqui MRH (2013) Green synthesis of silver nanoparticles mediated by Pulicaria glutinosa extract. Int J Nanomed 8:1507

Losurdo M, Giangregorio MM, Capezzuto P, Bruno G, Malandrino G, Fragalà IL, Armelao L, Barreca D, Tondello E (2007) Structural and optical properties of nanocrystalline Er2O3 thin films deposited by a versatile low-pressure MOCVD approach. J Electrochem Soc 155(2):G44

Mahnashi MH, Alqahtani YS, Alqarni AO, Alyami BA, Alqahtani OS, Jan MS, Hussain F, Islam ZU, Ullah F, Ayaz M (2022a) Phytochemistry, anti-diabetic and antioxidant potentials of Allium consanguineum Kunth. BMC Complement Med Ther 22(1):1–16

Mahnashi MH, Alyami BA, Alqahtani YS, Alqarni AO, Jan MS, Ayaz M, Ullah F, Rashid U, Sadiq A (2022b) Molecular docking supported observed changes in anticholinesterase, antioxidant and α-glucosidase inhibitions upon the bromination of benzene sulfonamide. Journal of the Chemical Society of Pakistan 44(1)

Mir NT, Saleem U, Anwar F, Ahmad B, Ullah I, Hira S, Ismail T, Ali T, Ayaz M (2019) Lawsonia inermis markedly improves cognitive functions in animal models and modulate oxidative stress markers in the brain. Medicina 55(5):192

Mohamed HEA, Afridi S, Khalil AT, Zia D, Iqbal J, Ullah I, Shinwari ZK, Maaza M (2019a) Biosynthesis of silver nanoparticles from Hyphaene thebaica fruits and their in vitro pharmacognostic potential. Mater Res Express 6(10):10509

Mohamed HEA, Afridi S, Khalil AT, Zohra T, Alam MM, Ikram A, Shinwari ZK, Maaza M (2019b) Phytosynthesis of BiVO 4 nanorods using Hyphaene thebaica for diverse biomedical applications. AMB Express 9(1):1–14

Mohamed HEA, Afridi S, Khalil AT, Zia D, Zohra T, Ali M, Alam MM, Shinwari ZK, Maaza M (2020) Phyto-fabricated Cr2O3 nanoparticle for multifunctional biomedical applications. Nanomedicine 15(17):1653–1669

Mohamed HEA, Afridi S, Khalil AT, Ali M, Zohra T, Akhtar R, Ikram A, Shinwari ZK, Maaza M (2020a) Promising antiviral, antimicrobial and therapeutic properties of green nanoceria. Nanomedicine 15(05):467–488

Mohamed HEA, Afridi S, Khalil AT, Ali M, Zohra T, Salman M, Ikram A, Shinwari ZK, Maaza M (2020b) Bio-redox potential of Hyphaene thebaica in biofabrication of ultrafine maghemite phase iron oxide nanoparticles (Fe2O3 NPs) for therapeutic applications. Mater Sci Eng, C 112:110890

Mohamed HEA, Afridi S, Khalil AT, Zia D, Shinwari ZK, Dhlamini MS, Maaza M (2020c) Structural, morphological and biological features of ZnO nanoparticles using Hyphaene thebaica (L) mart fruits. J Inorg Organomet Polym Mater 30(8):3241–3254

Mohamed H, Thema T, Dhlamini M (2021) Green synthesis of CuO nanoparticles via Hyphaene thebaica extract and their optical properties. Mater Today Proc 36:591–594

Mohammadi M, Fray D (2009) Development of nanocrystalline TiO2–Er2O3 and TiO2–Ta2O5 thin film gas sensors: controlling the physical and sensing properties. Sens Actuators B Chem 141(1):76–84

Munawar T, Yasmeen S, Hussain A, Akram M, Iqbal F (2020) Novel direct dual-Z-scheme ZnO-Er2O3-Yb2O3 heterostructured nanocomposite with superior photocatalytic and antibacterial activity. Mater Lett 264:127357

Nair SS, Kavrekar V, Mishra A (2013) In vitro studies on alpha amylase and alpha glucosidase inhibitory activities of selected plant extracts. Eur J Exp Biol 3(1):128–132

Nasar MQ, Shah M, Khalil AT, Kakar MQ, Ayaz M, Dablool AS, Shinwari ZK (2022) Ephedra intermedia mediated synthesis of biogenic silver nanoparticles and their antimicrobial, cytotoxic and hemocompatability evaluations. Inorg Chem Commun 137:109252

Nguyen T-D, Dinh C-T, Do T-O (2010) Shape-and size-controlled synthesis of monoclinic ErOOH and cubic Er2O3 from micro-to nanostructures and their upconversion luminescence. ACS Nano 4(4):2263–2273

NRC (1996) National Research Council Institute of laboratory animal resources, commission on life sciences.(1996). Guide for the care and use of laboratory animals

Ohlson L-O, Larsson B, Svärdsudd K, Welin L, Eriksson H, Wilhelmsen L, Björntorp P, Tibblin G (1985) The influence of body fat distribution on the

Mohamed *et al. AMB Express*   (2023) 13:24

Page 14 of 14

incidence of diabetes mellitus: 13 5 years of follow-up of the participants in the study of men born in. Diabetes 34(10):1055–1058

Ovais M, Khalil AT, Ayaz M, Ahmad I (2019) Biosynthesized metallic nanoparticles as emerging cancer theranostics agents Nanotheranostics. Springer, Berlin

Ovais M, Khalil AT, Ayaz M, Ahmad I (2020) Metal oxide nanoparticles and plants phytonanotechnology. Elsevier, Amsterdam

Ovais M, Hoque MZ, Khalil AT, Ayaz M, Ahmad I (2021) Mechanisms underlying the anticancer applications of biosynthesized nanoparticles Biogenic nanoparticles for cancer theranostics. Elsevier, Amsterdam

Pacio A, Santiago AC, Portillo MC, Díaz AR, Galicia CA, Pacio M, Moreno OP (2021) Visible upconversion of erbium oxide and their correlation with crystalline defects. Optik 240:166912

Pundir C, Aggarwal V (2017) Amperometric triglyceride bionanosensor based on nanoparticles of lipase, glycerol kinase, glycerol-3-phosphate oxidase. Anal Biochem 517:56–63

Que W, Buddhudu S, Zhou Y, Lam Y, Zhou J, Chan Y, Kam C, Gan L, Deen GR (2001) Preparation and characterization of erbium oxalate and erbium oxide nanoparticles by microemulsion technique. Mater Sci Eng, C 16(1–2):51–54

Radziuk D, Skirtach A, Geßner A, Kumke MU, Zhang W, Möhwald H, Shchukin D (2011) Ultrasonic approach for formation of erbium oxide nanoparticles with variable geometries. Langmuir 27(23):14472–14480

Rahim H, Sadiq A, Khan S, Amin F, Ullah R, Shahat AA, Mahmood HM (2019) Fabrication and characterization of glimepiride nanosuspension by ultrasonication-assisted precipitation for improvement of oral bioavailability and in vitro α-glucosidase inhibition. Int J Nanomed 14:6287

Rahimi-Nasrabadi M, Pourmortazavi SM, Karimi MS, Aghazadeh M, Ganjali MR, Norouzi P (2017) Statistical optimization of experimental parameters for synthesis of two efficient photocatalyst: erbium carbonate and erbium oxide nanoparticles. J Mater Sci: Mater Electron 28(20):15224–15232

Rajaji U, Manavalan S, Chen S-M, Chinnapaiyan S, Chen T-W, Ramalingam RJ (2019) Facile synthesis and characterization of erbium oxide (Er2O3) nanospheres embellished on reduced graphene oxide nanomatrix for trace-level detection of a hazardous pollutant causing methemoglobinaemia. Ultrason Sonochem 56:422–429

Sadiq A, Rashid U, Ahmad S, Zahoor M, AlAjmi MF, Ullah R, Noman OM, Ullah F, Ayaz M, Khan I (2020) Treating hyperglycemia from Eryngium caeruleum M Bieb: in-vitro α-glucosidase, antioxidant, in-vivo antidiabetic and molecular docking-based approaches. Frontiers Chem 8:558641

Saeed K, Ahmad S, Ahmad H, Ullah F, Sadiq A, Uddin A, Khan I, Ahmad M (2021) Green synthesis, characterization and cholinesterase inhibitory potential of gold nanoparticles. J Mex Chem Soc 65(3):416

Sani A, Hassan D, Khalil AT, Mughal A, El-Mallul A, Ayaz M, Yessimbekov Z, Shinwari ZK, Maaza M (2021) Floral extracts-mediated green synthesis of NiO nanoparticles and their diverse pharmacological evaluations. J Biomol Struct Dyn 39(11):4133–4147

Shaheen TI, El-Naggar ME, Hussein JS, El-Bana M, Emara E, El-Khayat Z, Fouda MM, Ebaid H, Hebeish A (2016) Antidiabetic assessment; in vivo study of gold and core-shell silver-gold nanoparticles on streptozotocin-induced diabetic rats. Biomed Pharmacother 83:865–875

Tabanli S, Eryurek G, Di Bartolo B (2017) White light emission from Er2O3 nanopowder excited by infrared radiation. Opt Mater 69:207–213

Wang G, Peng Z, Gong Z, Li Y (2018a) Synthesis, biological evaluation, and docking studies of novel 5, 6-diaryl-1, 2, 4-triazine thiazole derivatives as a new class of α-glucosidase inhibitors. Bioorg Chem 78:195–200

Wang X, Jiang Y-F, Liu Y-N, Xu A-W (2018b) Erbium oxide as a novel support for palladium nanocatalysts with strong metal–support interactions: remarkable catalytic performance in hydrogenation reactions. New J Chem 42(24):19901–19907

Zak AK, Majid WA, Abrishami ME, Yousefi R (2011) X-ray analysis of ZnO nanoparticles by Williamson-Hall and size–strain plot methods. Solid State Sci 13(1):251–256

Publisher's Note